

Destruction of potential vorticity by winds:  
implications for the formation of Eighteen Degree  
Water

Leif Thomas

*School of Oceanography, University of Washington  
Seattle, Washington*

John Marshall

*Program in Atmospheres, Oceans and Climate  
Department of Earth, Atmospheric and Planetary Sciences  
Massachusetts Institute of Technology  
Cambridge, Massachusetts*

August 22, 2005

# 1 Introduction

In this short article we:

1. Put forward a formation mechanism for EDW which involves the destruction of PV due to ‘down-front’ wind stress
2. Illustrate the mechanism in idealized and more realistic models
3. Discuss implications for the CLIMODE experiment
4. Suggest how one might make use of the observations to be collected in CLIMODE to test our hypothesis.

The article is set out as follows. In section 2 we present relevant background material that makes use of PV flux ideas. In section 3 we present our mode water formation hypothesis. In section 4 we test out the plausibility of our ideas with observations and a more realistic model of the Gulf Stream and its recirculation. In section 5 we briefly discuss the implication of these ideas for the observing program being deployed by CLIMODE and give our recommendations on how the observational strategy can be slightly modified so that the observations can also be used to test the mode water formation mechanism involving wind-forcing.

## 2 Background

The defining feature of EDW is that it is characterized by low potential vorticity (PV)  $q$

$$q = \omega_a \cdot \nabla b, \tag{1}$$

where  $\omega_a = f\hat{k} + \nabla \times \mathbf{u}$  is the absolute vorticity and  $b = -g\rho/\rho_o$  is the buoyancy. Formation of EDW therefore involves a modification and destruction of the PV. PV is changed by diabatic processes and by frictional forces. EDW formation has long been attributed to diabatic processes associated with convection driven by surface buoyancy loss. However, we argue here that it is possible that frictional forces driven by wind-stress also contribute to production of EDW. To quantify how important friction is in this process, it is instructive to consider PV dynamics and PV fluxes.

### 2.1 Potential vorticity fluxes

Useful insights in to EDW formation can be obtained by considering the flux form of the PV equation and its attendant theorems — see Haynes and McIntyre (1987) — discussed and applied in an oceanographic context, by Marshall and Nurser (1992) and Marshall et al. (2001). Changes in the PV result from convergences/divergences of the PV flux, i.e.

$$\frac{\partial q}{\partial t} = -\nabla \cdot \mathbf{J}, \tag{2}$$

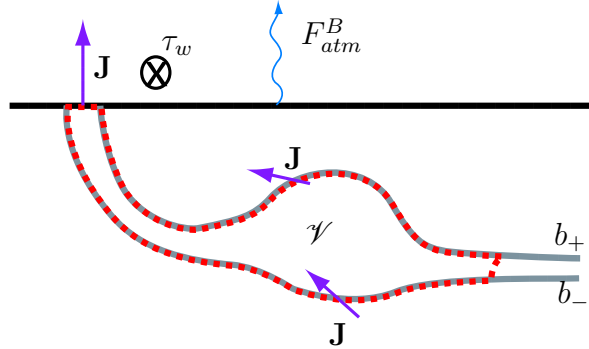


Figure 1: A control volume  $\mathcal{V}$  (dashed lines) with side surfaces coincident with isopycnals (gray contours) with buoyancy  $b_+$  and  $b_-$  that bound the EDW. The “down-front” wind-stress  $\tau_w$  and flux of buoyancy from the ocean to the atmosphere  $F_{atm}^B$  will result in an upward PV flux  $\mathbf{J}$  at the sea-surface.

where the PV flux

$$\mathbf{J} = q\mathbf{u} + \nabla b \times \mathbf{F} - \mathcal{D}\boldsymbol{\omega}_a \quad (3)$$

has an advective constituent  $q\mathbf{u}$  and nonadvective constituents that arise from diabatic processes  $\mathcal{D}$ :

$$\mathcal{D} \equiv \frac{\partial b}{\partial t} + \mathbf{u} \cdot \nabla \mathbf{b} \quad (4)$$

and from frictional forces  $\mathbf{F}$ .

To determine what atmospheric forcing conditions are favorable for PV destruction and whether or not friction can play a significant role in EDW formation, consider integrating (2) over a control volume that encircles the EDW. Application of Gauss’ theorem to the integral reveals that reduction of the volume-averaged PV occurs when the net flux of PV through the surface of the control volume is outward. Consider the control volume  $\mathcal{V}$  shown in Fig.1, with an upper surface that coincides with the frontal outcrop window of the EDW, side surfaces that are the isopycnals bounding the EDW, and a bottom surface that crosses isopycnals at a depth where the flow, frictional forces, diabatic processes and hence PV fluxes are weak. For such a volume, only the PV flux out of the sea-surface contributes to the change of volume-averaged PV since no PV is fluxed through the isopycnal surfaces of the control volume, in accordance with the “impermeability theorem” of Haynes and McIntyre (1987). Therefore, the PV in the control volume will be reduced if the PV flux at the sea-surface is upward. Note that this PV flux perspective may provide a considerable simplification over that due to Walin (1982) because, unlike PV, buoyancy does not have an impermeability theorem and so, in the Walin framework, to reconcile formation and subduction rates, account must be taken of dissipative processes. Indeed the conundrum of balancing EDW formation and dissipation rates is at the heart of the Climode project — see Marshall (2005).

At the sea-surface, in the limit of a rigid lid, the vertical velocity is zero or otherwise weak so that the vertical component of the PV flux is dominated by its nonadvective

constituents. Under what atmospheric forcing condition is the nonadvective PV flux at the surface upward? For an inertially stable flow, where  $f(f + \hat{k} \cdot \nabla \times \mathbf{u}) > 0$ , diabatic processes will result in an upward PV flux

$$J_z^{\mathcal{D}} = -(f + \hat{k} \cdot \nabla \times \mathbf{u})\mathcal{D} \quad (5)$$

when  $\mathcal{D} < 0$  (i.e. cooling). Diabatic processes will reduce the buoyancy, i.e.  $\mathcal{D} < 0$ , when there is a net loss of buoyancy from the ocean to the atmosphere, i.e.  $F_{atm}^B > 0$ . This result that PV destruction and mode water formation occurs when  $F_{atm}^B > 0$  is not surprising, since buoyancy loss to the atmosphere triggers convective mixing which reduces the stratification.

The vertical component of the nonadvective PV flux associated with frictional forces

$$J_z^F = \nabla_h b \times \mathbf{F} \quad (6)$$

is nonzero only if there is a horizontal buoyancy gradient  $\nabla_h b$ . Associating the horizontal buoyancy gradient with a vertically sheared geostrophic flow  $\mathbf{u}_g$  via the thermal wind relation

$$\nabla_h b = f \frac{\partial \mathbf{u}_g}{\partial z} \times \hat{k}$$

reveals that the nonadvective PV flux associated with frictional forces

$$J_z^F = f \frac{\partial \mathbf{u}_g}{\partial z} \cdot \mathbf{F} \quad (7)$$

is upward when the frictional force is in the direction of the geostrophic shear. For wind-forced flows, the frictional force is dominantly in the direction of the wind-stress. Currents at upper-ocean fronts such as the Gulf Stream are usually surface intensified so that the surface current of the front is oriented with the geostrophic shear. Therefore, when the wind blows in the direction of the frontal jet, i.e. is in a “down-front” orientation, the conditions are favorable for PV destruction by wind forces (i.e.  $J_z^F > 0$ ).

## 2.2 Relative importance of buoyancy loss and wind-stress in destroying PV

In the previous section, it has been shown that both buoyancy loss and “down-front” winds lead to destruction of PV. The question arises: what are the relative contributions of these two types of atmospheric forcing at destroying PV and forming EDW? To address this issue, consider the following scaling argument. Under conditions of atmospheric buoyancy loss, gravitational instability will result in a convective buoyancy flux that scales with the buoyancy loss to the atmosphere  $F_{atm}^B$  and that decays nearly linearly with depth through the mixed layer of thickness  $H$  Large et al. (1994). Therefore an appropriate scale for diabatic processes induced by buoyancy loss to the atmosphere is  $\mathcal{D} \sim F_{atm}^B/H$ , so that the scaling for (5) is

$$J_z^{\mathcal{D}} \sim f \frac{F_{atm}^B}{H}. \quad (8)$$

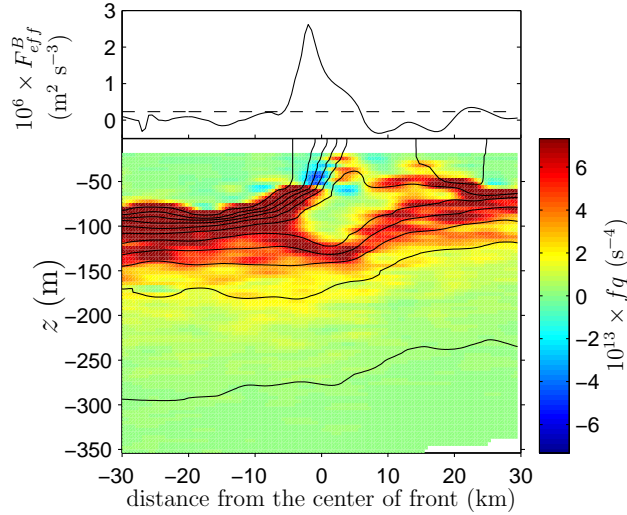


Figure 2: Lower panel: cross-sections of density (black contours) and the two-dimensional PV at the subpolar front of the Japan/East Sea during a cold-air outbreak on January 31, 2000. The contour interval of the density field is  $0.1 \text{ kg m}^{-3}$ . Upper panel: lateral structure of the wind-driven buoyancy flux (solid) and the buoyancy loss to the atmosphere (dashed), the later being equivalent to a heat loss of  $490 \text{ W m}^{-2}$ .

A wind-stress of strength  $\tau_o$  will exert a frictional force of scale  $F \sim \tau_o/\rho_o\delta_e$  over the turbulent Ekman layer of thickness  $\delta_e = 0.4u^*/f$ , where  $u^* = \sqrt{\tau_o/\rho_o}$  is the friction velocity Wimbush and Munk (1970). If the magnitude of the horizontal buoyancy gradient at the front is  $S^2 = |\nabla_h b|$ , then the appropriate scaling for (6) is

$$J_z^F \sim S^2 \frac{\tau_o}{\rho_o\delta_e}. \quad (9)$$

The relative contributions of friction and diabatic effects to PV reduction can be assessed by taking the ratio of (9) and (8)

$$\frac{J_z^F}{J_z^{\mathcal{D}}} \sim \left(\frac{H}{\delta_e}\right) \left(\frac{F_{wind}^B}{F_{atm}^B}\right), \quad (10)$$

where  $F_{wind}^B = \mathbf{M}_e \cdot \nabla_h b \sim S^2\tau_o/\rho_o f$  is the “wind-driven buoyancy flux” (WDBF), and  $\mathbf{M}_e$  is the Ekman transport. For “down-front” winds, Ekman flow advects water from the dense side of the front over lighter waters, triggering convection. What the WDBF physically represents is the scaling for the convective buoyancy flux associated with this Ekman-driven convection Thomas and Lee (2005).

On account of the strong lateral density gradients, at wind-forced fronts, the WDBF can be comparable or larger than the atmospheric buoyancy loss, making the ratio (10) greater than or equal to one. This even holds at subpolar fronts in the northern hemisphere forced by wintertime cold-air outbreaks that extract large amounts of heat from the ocean yet also force the fronts strongly with “down-front” wind-stress. For example, using hydrographic

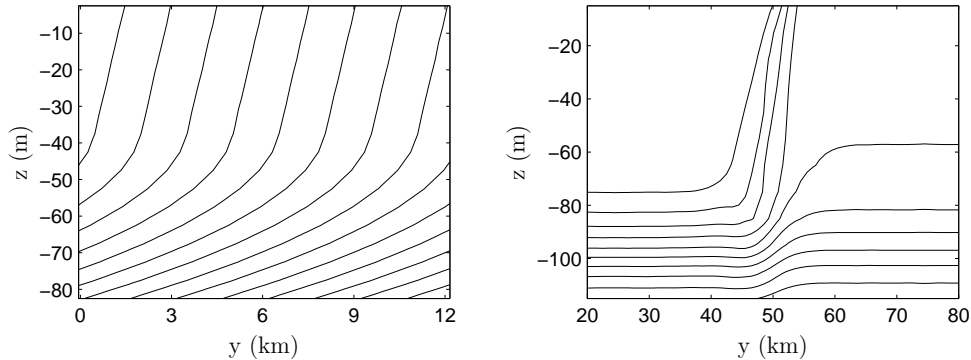


Figure 3: Initial density field for the 2-D frontal zone experiments (left) and the 3-D isolated front experiment. The contour interval is  $0.1 \text{ kg m}^{-3}$ . Both experiments were forced by a spatially-uniform wind-stress blowing out of the page. A corresponding geostrophic flow accompanies the density field.

measurements combined with shipboard meteorological data taken at the subpolar front of the Japan/East Sea during a cold-air outbreak Thomas and Lee (2005) estimated the WDBF to be an order of magnitude larger than the atmospheric buoyancy flux even with the heat loss of  $490 \text{ W m}^{-2}$  experienced at the front, see Fig. 2. This implies that the ratio (10) was of order 10 at the front, and suggests that PV destruction by winds dominated over that due to surface cooling during the cold-air outbreak. We will present evidence in Section 4 that  $J_z^F/J_z^{\mathcal{D}} \sim 10$  in the Climode region.

The low PV at the core of the front shown in Fig. 2 is evidence that PV destruction has occurred. Notice that the PV at the front is zero to negative while the stratification is stable. Although it may seem somewhat paradoxical that the fluid has zero to negative PV yet non-zero stratification, it must be realized that for a strongly baroclinic current such as that associated with a front, the horizontal vorticity (i.e. vertical shear) and horizontal buoyancy gradients significantly contribute to the PV (1), so that the combined conditions of  $q \leq 0$  and  $\partial b/\partial z > 0$  can be met if  $f\omega_a \cdot \nabla_h b < 0$ , a condition that is always satisfied for a geostrophically-balanced current. Fluid that has low PV owing to its baroclinicity and not its stratification will be referred to as having “baroclinically-low” PV. The idea that convection sets PV, rather than stratification, to zero is discussed in Haine and Marshall (1998) and Marshall and Schott (1999).

### 2.3 Idealized numerical experiments

In the previous section, it was shown that forcing of fronts by “down-front” winds leads to a reduction of the volume-averaged PV. To study the details of this process, two and three dimensional numerical experiments of idealized fronts forced by “down-front” winds were performed, the initial conditions of which are shown in Fig. 3.

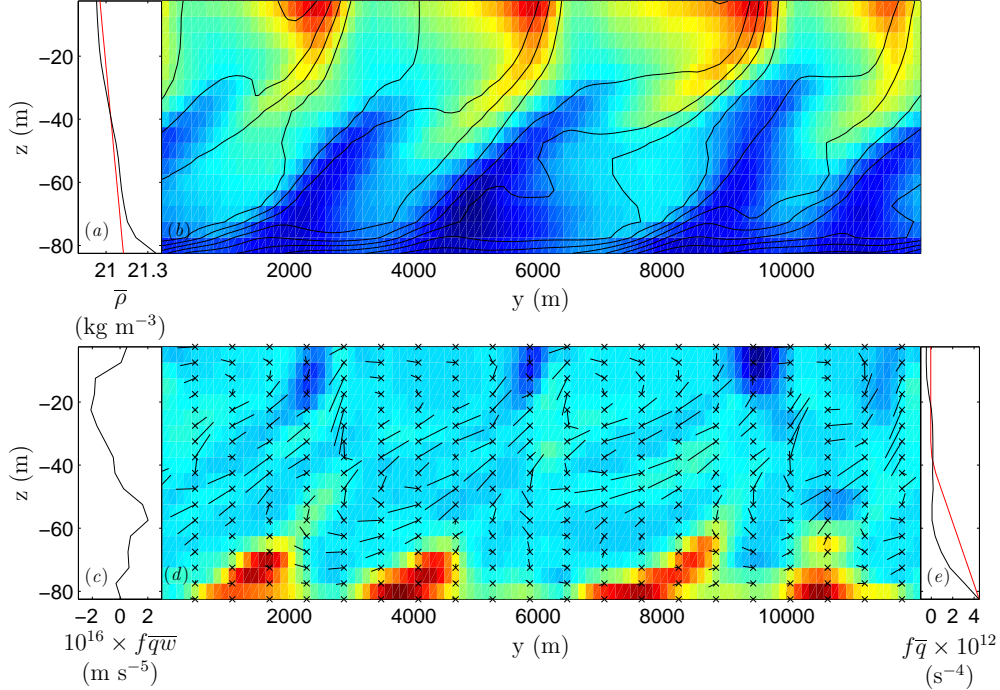


Figure 4: Solutions from the 2-D experiment at  $t = 8.6$  inertial periods. (a) The meridionally averaged density (black) compared to a density field with a constant stratification of  $S^4/f^2$  (red); (b) zonal velocity (shades) and density (contours) fields; (c) the meridionally averaged advective PV flux; (d) PV (shades) and secondary circulation (vectors); and (e) the meridionally averaged PV at  $t = 0$  (red) and  $t = 8.6$  (black) inertial periods. In both (b) and (d), warm (cool) shades indicate higher (lower) values.

### 2.3.1 Two-dimensional frontal zone experiment

The 2-D experiment was configured to represent an idealized frontal zone with a spatially-uniform lateral buoyancy gradient of strength  $S^2 = -\partial\bar{b}/\partial y$  (where  $\bar{b} = (1/L) \int_0^L b dy$  and  $L = 12$  km is the width of the domain), for more details of the experiment see Thomas (2005). For the experiment, in a surface layer of thickness  $H$ , the stratification  $N_{ml}^2$  is constant and non-zero yet the PV  $q = fN_{ml}^2 - S^4$  is nearly zero owing to the strong baroclinicity of the frontal zone. Beneath this surface layer, there is a pycnocline with high PV. To isolate the process of PV destruction by friction, the frontal zone is forced by a spatially-uniform “down-front” wind-stress of magnitude  $0.1 \text{ N m}^{-2}$ , while the surface buoyancy flux is set to zero.

A solution representative of the numerical experiment is shown in Fig. 4. As illustrated in the meridional section of the density and zonal velocity (Fig. 4b), forcing of the frontal-zone by “down-front” winds leads to the formation of multiple fronts with sharp, frontal jets. The fronts form within several inertial periods as a result of frontogenetic secondary circulations characterized by upwelling along the frontal interface and downwelling of the Ekman flow (i.e. southward flow in the upper 20 m in between the fronts) down the dense side of the front, Fig. 4d. As evident in Fig. 4d, the secondary circulation is most intense

above the strongly-stratified pycnocline, yet exists in a region where the stratification of the meridionally averaged density  $\bar{\rho}$  is non-zero (Fig. 4a). The region that the overturning motions occupy is therefore not characterized by a homogeneous density layer as with typical mixed layers, but is characterized by a “zero-PV layer” with a “baroclinically-low”, nearly-zero meridionally-averaged PV (Fig. 4e).

The “zero-PV layer” deepens with time, as high PV is eroded from the pycnocline (Fig. 4e). This erosion of PV indicates a net reduction of the total PV in the domain, a result that was to be expected since frictional forces by “down-front” winds drive a net PV flux out of the surface of the ocean and hence reduce the volume averaged PV. PV destruction occurs at the base of the “zero-PV layer” and not within the Ekman layer ( $\delta_e \approx 40$  m) where frictional forces are expected to be largest, therefore, it is not obvious that friction is directly responsible for the fluxing of PV out of the pycnocline and the deepening of the layer. What is responsible for the deepening of the layer is the advective PV flux associated with the secondary circulations. The way in which the secondary circulation reduces the PV of the pycnocline is illustrated in Fig. 4d. Near the base of the “zero-PV layer”, upward motions advect high PV from the pycnocline while downward motions draw low-PV waters from the surface into the pycnocline. This leads to a positive correlation between the PV and the vertical velocity, yielding an upward advective PV flux  $\overline{qw} > 0$  (Fig. 4c) that extracts PV from the pycnocline and deepens the “zero-PV layer.” Although the frictional nonadvective PV flux does not play a major role at the base of the “zero-PV layer”, in the Ekman layer it is critical. Near the surface, the frictional PV flux leads to a PV flux divergence that maintains the low PV values in the Ekman layer. This frictionally-induced source of low PV is necessary to sustain the deepening of the “zero-PV layer”, since the secondary circulation acts only to exchange PV vertically and therefore cannot decrease the volume-averaged PV of the frontal zone.

### 2.3.2 Three-dimensional isolated front experiment

The 2-D numerical experiment discussed above shows how “down-front” winds result in the formation of a surface layer with low-PV, yet the experiment still leaves unclear how PV destruction can lead to EDW formation, since the fluid in the “zero-PV” layer is stratified and hence is distinct from the weakly stratified waters commonly associated with EDW. As illustrated in the 3-D numerical experiment presented below, what is necessary to make the connection between PV destruction by winds and EDW formation is the meandering and eddying motions of the front.

In contrast to the 2-D frontal zone experiment, the 3-D experiment was configured with an isolated front, Fig.3, characterized by properties representative of the subpolar front of the Japan/East Sea. The experiment shows how several inertial periods after the initialization of the “down-front” wind forcing, the front becomes unstable to 3-D instabilities (Fig.5). To see a movie of the experiment go to

[http://www.ocean.washington.edu/people/faculty/leif/PVsurf\\_mov.gif](http://www.ocean.washington.edu/people/faculty/leif/PVsurf_mov.gif)

The vertical circulation associated with the meandering of the front draws the “baroclinically-

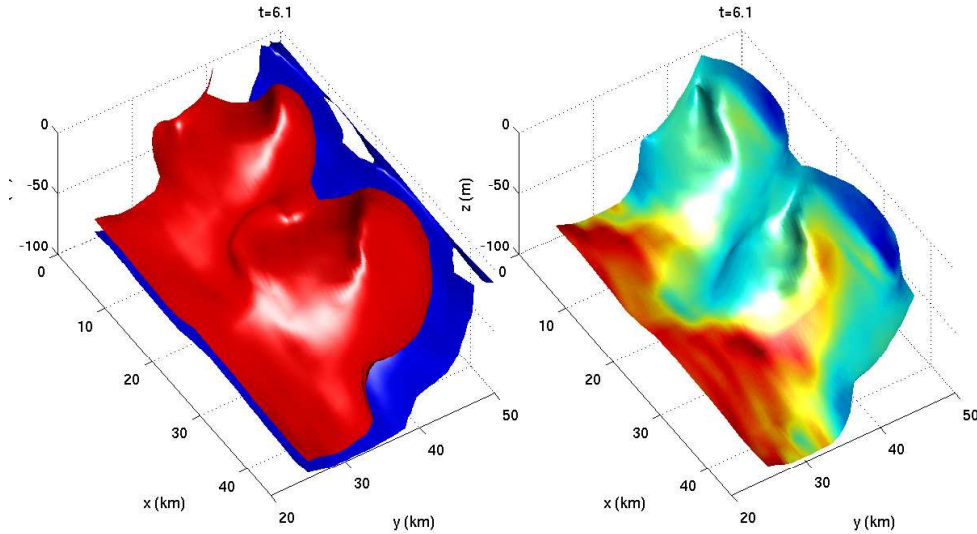


Figure 5: Solutions from a 3-D experiment of a front at  $t = 6.1$  inertial periods after a spatially-uniform, “down-front” wind-stress was turned on. Left panel: isopycnal surfaces that bound the frontal zone. Right panel: PV on the isopycnal surface that lies inbetween the two isopycnals shown to the left. The frontal jet is flowing in the positive  $x$ -direction.

low” PV water from the core of the front down and to the south of the front, pooling the low-PV water into anticyclonic eddies. As the low-PV water is subducted, the isopycnal surfaces surrounding this water spread apart laterally and vertically creating a bolus of weakly stratified water, more reminiscent of EDW. What has occurred during the subduction of the frontal water is a conversion of the “flavor” of PV of the fluid from being “baroclinically-low” with  $q = fN^2 - f(\partial u/\partial z)^2 \approx 0$  to being weakly stratified with  $q = fN^2 \approx 0$ . Notice in the plot of the PV in Fig.5 that the lowest PV in the domain is found at the core of the front near the surface where the lateral buoyancy gradient is strongest. This is the region where the frictional PV flux (6) is most intense, and hence is the where the low-PV water is actively being formed. Once formed, the low-PV water is advected down-stream and subducted, generating the weak stratification to the south of the front. This implies that the formation of the boluses of weakly stratified water to the south of the front is a non-local process: that is, it is the PV fluxes at the core of the front and not the local surface PV fluxes to the south of the front that are responsible for the low-PV water found there. This leads us to postulate that while local heat loss to the south of the Gulf Stream may contribute to the formation of EDW, EDW may also be formed in the core of the Gulf Stream and transmitted isopycnally into the Southern recirculation gyre by eddies. This process would involve eddy PV fluxes. We see evidence for such eddy PV fluxes in the right panel of Fig.5, i.e. low (high) PV fluid is correlated with the downward (upward), along-isopycnal, circulation of the eddy, yielding a net upward eddy PV flux, in the same direction as the surface frictional PV flux that forces the front.

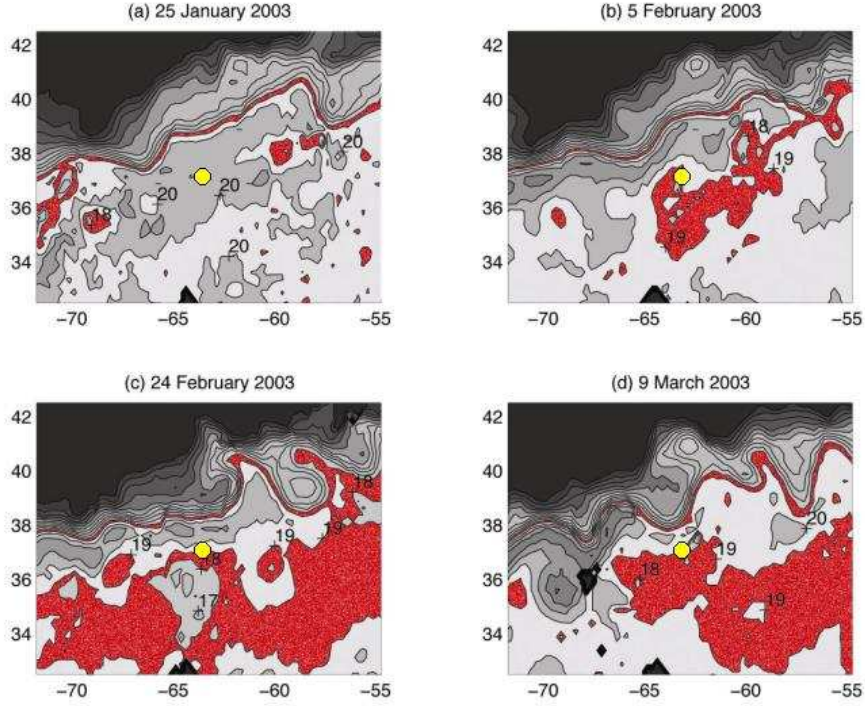


Figure 6: Wintertime SST from the AMSR-E microwave sensor, courtesy of Remote Sensing Systems. The  $17^{\circ}$ -to- $19^{\circ}$  C outcrop window is colored red. Note the warm core of the Gulf Stream and the irregular opening of the EDW ventilation window (classically between about  $17.5^{\circ}$  and  $18.5^{\circ}$  C).

### 3 Proposed mechanism for formation of EDW

#### 3.1 Hypothesis

Based on the PV flux arguments and numerical experiments presented above, we hypothesize that it is the part of the  $17^{\circ} - 19^{\circ}$  outcrop window that encircles the core of the Gulf Stream that is crucial to the formation of EDW, because it is here where the lateral buoyancy gradient and hence the wind-driven buoyancy flux is largest. This is clearly visible in Fig.6. In this region, both buoyancy loss and the “down-front” wind-stress destroy the PV and create a plug of “baroclinically-low” PV. This low PV is advected down-stream until the front forms a southward turning meander/anticyclone. Ageostrophic flow associated with the meander/eddy subducts the low PV, driving the low PV fluid downward and equatorward. As the low PV is drawn off the front, the “baroclinically-low” PV is converted to a low-stratification type PV, i.e. the type of low PV associated with EDW. In this flavor-of-PV conversion process, the isopycnal surfaces bounding the low PV water spread apart, and reduce the stratification. It is possible that during this process, on the southward journey of the low PV, the upper isopycnal surface punches through the sea surface and exposes the EDW to the atmosphere. This is a non-local process, i.e. the

weak stratification found south of the front may not be a consequence of local atmospheric buoyancy loss, but rather a consequence of the buoyancy loss and “down-front” wind-stress forcing found upstream in the core of the Gulf Stream that destroy the PV.

We also hypothesize that calculating a PV budget on the isopycnal layer surrounding the EDW may provide a more accurate estimate of the formation rate of EDW as compared to estimates made using isopycnal volume budgets via the Walin framework. In contrast to the volume budget of an isopycnal layer where diapycnal volume and diffusive fluxes on the interior isopycnal surfaces bounding the layer must be considered, owing to the impermeability theorem, the PV fluxes on these interior isopycnal surfaces do not contribute to the PV budget and therefore do not need to be measured. The implication being, only the PV flux at the sea-surface (that we might have a hope of observing) must be estimated to perform the PV budget, which makes the book-keeping for the PV budget easier and eliminates errors that might arise from uncertainties in estimates of the interior fluxes. What we would like to know, however, is not the PV flux, but the volume flux of the newly formed EDW. In a similar manner to that described in Marshall and Nurser (1992), this can be accomplished by converting the surface PV flux to a subduction rate for the EDW by dividing the PV flux by the PV contrast between the EDW and the pycnocline.

### 3.2 Testing the hypothesis

To test this hypothesis it will be necessary to evaluate the components of  $J_z$  at the sea surface, i.e. calculate (5) and (6), in the EDW outcropping window. This will involve monitoring synoptic patterns of the sea-surface buoyancy field, surface wind-stress, air-sea heat flux, mixed-layer depth, and Ekman layer depth. The estimates of the surface PV flux will be used to determine:

1. If the core of the Gulf Stream is the region where the PV is being destroyed and EDW is formed
2. Whether “down-front” winds or buoyancy loss dominates the EDW formation process
3. What is the formation rate of EDW.

Another aspect of the hypothesis that needs to be tested is the non-local behavior of the formation of the EDW. This would best be accomplished using Lagrangian measurements tracking water originating from the core of the Gulf Stream. What would be ideal would be to measure the stratification and vertical shear on a Lagrangian platform so as to observe the conversion of the low-PV fluid’s flavor (where  $q \approx fN^2 - f(\partial u/\partial z)^2 \approx 0$  water converts to  $q \approx fN^2 \approx 0$  water) and to monitor its subduction and subsequent evolution. If Lagrangian measurements of the vertical shear are not possible, measurements of a tracer that characterizes frontal waters and that is obtainable from hydrography, “spice” for example, could be used as a proxy for the PV and followed in its journey along the Stream to see if it is accumulated in pools of EDW south of the front.

## 4 Preliminary calculations testing feasibility of proposed mechanism

In addition to collecting new field observations in the CLIMODE program, preliminary observations and models can be analyzed to address the ideas set out in the previous sections. In particular, several rather straightforward calculations can be made to test the feasibility of the proposed mechanism. We present some ideas and preliminary results here.

### 4.1 Analysis of data

The first set of calculations would involve analyzing remote sensing data from previous winters to assess the impact that “down-front” wind forcing might have on the formation of EDW. Maps of SST and wind-stress can be used to estimate the wind-driven buoyancy flux  $F_{wind}^B = \mathbf{M}_e \cdot \nabla_h b$  or in more familiar units a wind-driven heat flux

$$F_{wind}^Q = \rho_o C_w \mathbf{M}_e \cdot \nabla_h T, \quad (11)$$

where  $C_w$  is the specific heat of water (note that for more accurate calculations, the density compensating effect of the salinity should be taken into account). Comparing the magnitude of the wind-driven heat flux to heat loss estimates over the Gulf Stream will tell us qualitatively if “down-front” winds are a key element to EDW formation.

We have performed a preliminary calculation along these lines to estimate the relative magnitudes of the surface frictional and diabatic PV fluxes in the CLIMODE region for December 15th, 2003 (Fig.7). The calculation was performed as follows. An atmospheric boundary layer scheme driven by NCEP analyzed winds, temperatures and specific humidities, was employed which used bulk formulae, along with daily AMSR-E microwave sensor data, to compute air-sea heat fluxes and wind-stresses. The wind-driven heat flux (11) was estimated using the wind stress to calculate the Ekman transport and the SST to calculate the SST gradient. The calculation reveals that at the crest of the meander centered at around 40 N and 65 W, where wind-stress is “down-front”, in the EDW outcropping window, the wind-driven heat flux is several times larger than the air-sea heat flux. Assuming that the Ekman and mixed-layer depths are comparable in magnitude, this implies that the ratio of the surface frictional and diabatic PV fluxes (10) in the crest of the meander is greater than one, and suggests that PV destruction by winds can be a significant contributor to EDW formation.

It may also be possible to use the remote sensing data to see if EDW formation involves non-local processes. This would involve a variation on the advection-diffusion model driven by altimetric observations proposed by Marshall et al. (2005). The idea would be to flux in a tracer representing low-PV fluid into the surface of the ocean at a rate proportional to  $J_z^F$  (which has been estimated from the SST and wind fields), then use the velocity field derived from satellite altimetry to advect the tracer and follow it along its trajectory to see if it forms pools in the southern recirculation gyre at meanders and eddies in the front.

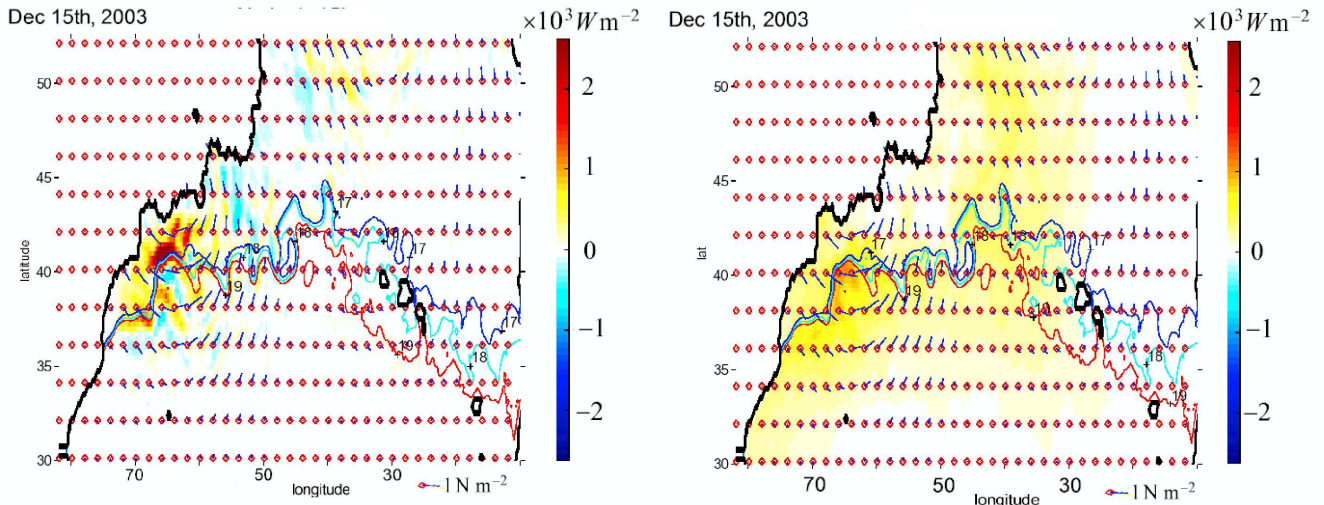


Figure 7: Estimation of the wind-driven heat flux (11) (left) and the air-sea heat flux (right), with positive values indicating oceanic heat loss, on December 15th, 2003 from observed SST and NCEP analyzed winds, temperatures, and specific humidities. The plots show the 17, 18 and 19 degree outcrops (contours) along with the surface wind stress (vectors) and the heat fluxes colored. The scale in the plots is the same. Figure courtesy of Ivana Cerovecki (MIT).

## 4.2 Diagnosis of a high resolution model of the Gulf Stream and its recirculation

We now present some preliminary calculations from a high resolution ( $\frac{1}{8}^\circ$ ) simulation of the ocean that has been set up in support of Climode by the MIT/JPL groups. The model, run by Dimitris Menemenlis (JPL) and Chris Hill (MIT), has 50 vertical levels (with 10 m vertical resolution in the top 150 m or so) and employs a KPP scheme (Large et al., 1994). It is driven by an atmospheric boundary layer scheme in which NCEP analyzed surface winds, temperatures and specific humidities are used, along with the evolving SST field from the model, to compute air-sea heat fluxes.

From Fig.8a we see that, on this particular occasion<sup>1</sup> — March, 8th, 2001 — the Gulf Stream is meandering to the south of its climatological position, throwing off cold and warm rings. There is an atmospheric cyclone centered over the Stream with winds directed along the Gulf Stream front. The air-sea heat flux, Fig.8b, shows a clear imprint of SST variations associated with the underlying meandering Gulf Stream. The mixed layer depth reaches down to 100-150 m or so and is clearly strained and teased out by mesoscale variability. The wind-driven heat flux (11) is plotted in Fig.8c and is a measure of the vertical component of the PV flux at the sea surface due to the windstress,  $J_z^F$ .

<sup>1</sup>We have no expectation that the ocean model will capture the observed position of the Gulf Stream and its rings and eddies on any particular occasion. The model is driven by analyzed atmospheric field, but is not constrained by in-situ ocean observations.

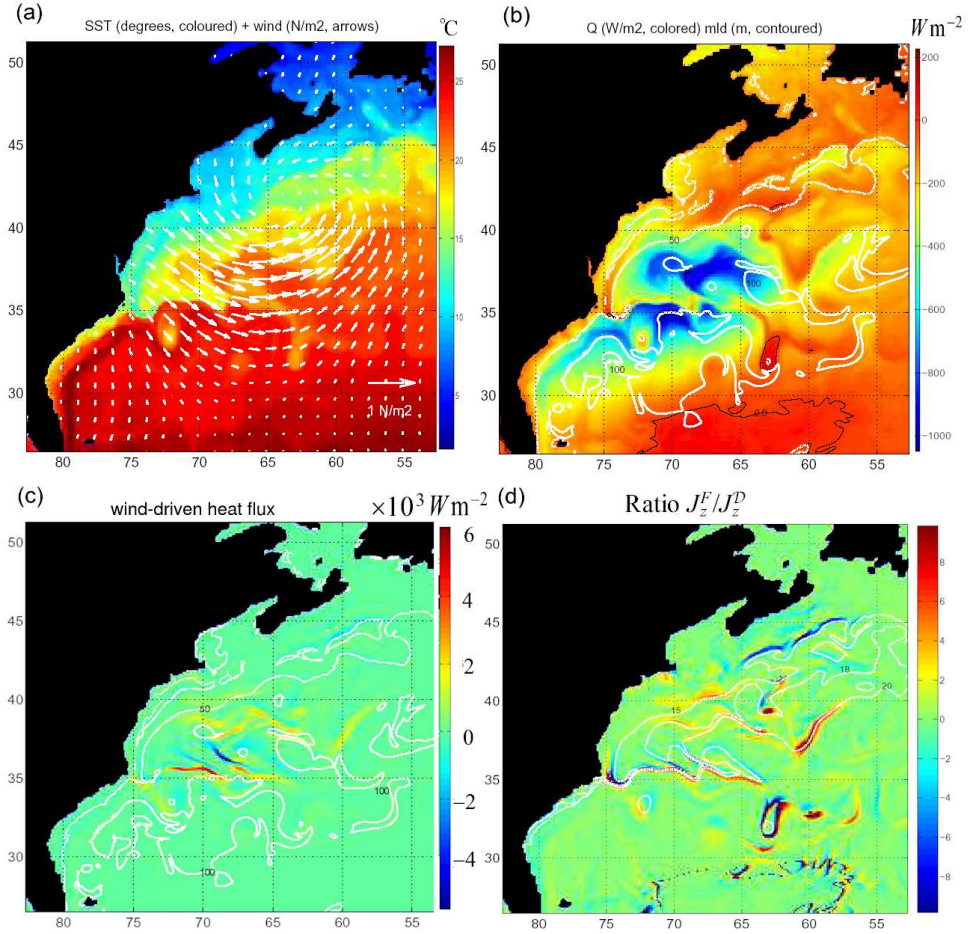


Figure 8: Diagnoses of air-sea interaction in a high resolution ( $\frac{1}{8}^\circ$ ) simulation of the ocean using the MITgcm. The configuration is global — only the Gulf Stream and its recirculation is shown here. All fields are averages from March 8th 2001. (a) Surface wind-stress and SST (b) net air-sea heat flux (colored), negative values indicate oceanic heat loss, and mixed layer depth (contoured) (c) the wind-driven heat flux (11) (colored), positive values indicate regions where PV destruction by winds is likely to be occurring, and the mixed layer depth (contoured) (d) the ratio of mechanical to diabatic non-advective PV flux at the sea surface, Eq.(10).

Red is a flux out of the ocean, indicating a tendency to create low PV fluid. We see it is concentrated in regions where, simultaneously, one observes strong frontal gradients and down-front winds (see Fig.8a). The ratio of mechanical to diabatic non-advective PV flux at the sea surface, Eq.(10), is plotted in Fig.8d. The ratio was calculated assuming that the Ekman and mixed-layer depths are of the same magnitude. In accord with the scaling presented in Section 2.2, the destabilization due to wind-stress exceeds that due to air-sea heat loss by a factor of 10 in strong frontal regions.

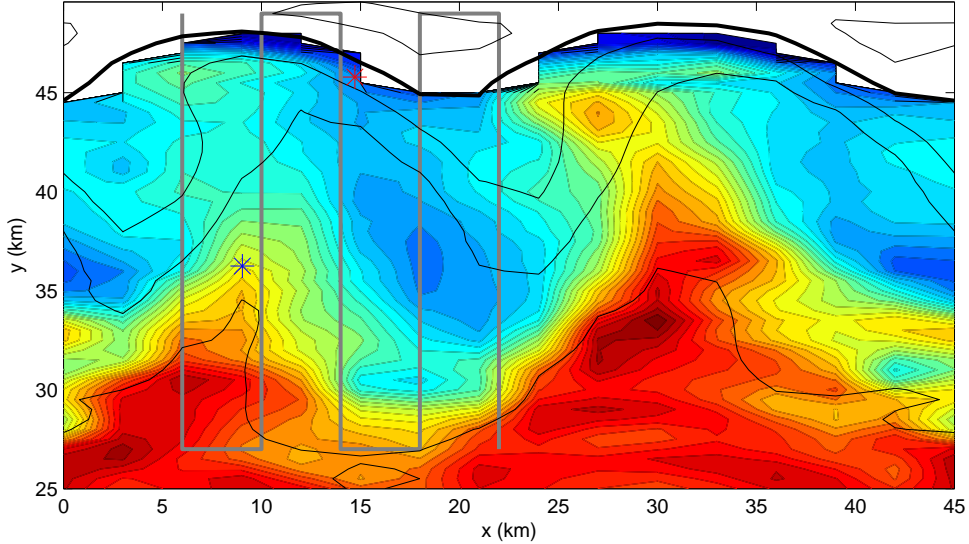


Figure 9: Possible SeaSoar tracklines (gray) and float deployment locations (asterisks) relative to a meander crest, illustrated using the surface density field (black contours) and isopycnal PV field (color) from the idealized 3-D experiment. The recommended location to deploy floats for tagging subducting (upwelling) water is marked with the red (blue) asterisk. The SeaSoar survey pattern is chosen to sample the stream of low-PV (high-PV) subducting (upwelling) downstream (upstream) of the meander crest. The isopycnal surface on which the PV is plotted, outcrops at the front along the line marked by the thick black contour.

## 5 Recommendations

To test the hypothesis that the core of the Gulf Stream is a region where EDW is formed and subsequently subducted, a combination of Lagrangian measurements using floats and Eulerian measurements of the PV field obtained from SeaSoar hydrography and shipboard ADCP currents would be ideal. If a few of the floats deployed during the wintertime survey cruises could be released in the core of the Gulf Stream, on the outcropping isopycnal within the EDW, and at a location/time where/when there are strong “down-front” winds, it might be possible to tag and track recently formed “baroclinically-low” PV water. Following the three-dimensional trajectories of the floats, one could assess whether there is a direct path linking the low-PV frontal waters and the weakly stratified EDW to the south of the Gulf Stream to determine if the front is a source of EDW. Maps of the PV and tracers tagging frontal water (such as spice) on the EDW isopycnal, obtained from SeaSoar and shipboard ADCP surveys, could also yield information connecting EDW and frontal waters. The question arises as to where would be the most ideal locations for the float deployments and SeaSoar surveys. We use the solutions from the idealized 3-D experiments as a first guess at answering this question. The experiments show that the “baroclinically-low” PV water is formed at the crests of meanders then subducted downstream of the crest. Hence, the best location to tag subducting low-PV water is just on

the downstream side of the crest, see Fig. 9. If one wanted to track the upwelled, relatively high-PV water, floats could be deployed upstream of a meander trough. These locations of preferred upwelling and downwelling upstream and downstream of a meander crest have been observed in the Gulf Stream using RAFOS floats (Bower and Rossby, 1989). Therefore, based on the RAFOS float observations and the numerical experiments, we recommend the following strategy. During the wintertime survey, use satellite SST and wind products to identify meander crests where PV destruction by winds is likely to be active (as in Fig. 7). At these meanders, deploy a few floats in the EDW isopycnal layer on the downstream side of the meander crest where subduction is likely. Finally, similar to what has already been planned, perform SeaSoar surveys that cover the meander crest and front, and extend to the adjacent troughs and south into the EDW region (Fig.9). The float velocities and vertical velocities inferred using the omega equation diagnostics could be used to estimate subduction rates. To determine if the surface PV flux is a useful metric for determining the formation rate of EDW, this subduction rate could be compared with that calculated using the method described in section 3.1 involving the surface PV flux and the EDW-pycnocline PV contrast.

## References

- Bower, A. S. and Rossby, T. (1989). Evidence of cross-frontal exchange processes in the Gulf Stream based on isopycnal RAFOS float data. *J. Phys. Oceanogr.*, 19:1177–1190.
- Haine, T. W. N. and Marshall, J. (1998). Gravitational, symmetric, and baroclinic instability of the ocean mixed layer. *J. Phys. Oceanogr.*, 28:634–658.
- Haynes, P. and McIntyre, M. (1987). On the evolution of vorticity and potential vorticity in the presence of diabatic heating and frictional or other forces. *J. Atmos. Sci.*, 44.
- Large, W. G., McWilliams, J. C., and Doney, S. C. (1994). Oceanic vertical mixing: a review and a model with a nonlocal boundary layer parameterization. *Rev. Geophys.*, 32:363–403.
- Marshall, J. (2005). Climode: a mode water dynamics experiment in support of clivar. *Clivar Variations*, 3(2):8–14.
- Marshall, J., Nilsson, J., and Jamous, D. (2001). Entry, flux and exit of potential vorticity in ocean circulation. *J. Phys. Oceanogr.*, 31:777–789.
- Marshall, J. and Schott, F. (1999). Open ocean deep convection: observations, models and theory. *Rev. Geophys.*, 37:1–64.
- Marshall, J., Shuckburgh, E., Jones, H., and Hill, C. (2005). Estimates and implications of surface eddy diffusivity in the southern ocean derived from tracer transport. *J. Phys. Oceanogr.* (submitted).
- Marshall, J. C. and Nurser, A. J. G. (1992). Fluid dynamics of oceanic thermocline ventilation. *J. Phys. Oceanogr.*, 22:583–595.
- Thomas, L. N. (2005). Destruction of potential vorticity by winds. *J. Phys. Oceanogr.* in press.
- Thomas, L. N. and Lee, C. M. (2005). Intensification of ocean fronts by down-front winds. *J. Phys. Oceanogr.*, 35:1086–1102.
- Walín, G. (1982). On the relation between sea-surface heat flow and thermal circulation in the ocean. *Tellus*, 34:187–195.
- Wimbush, M. and Munk, W. (1970). The benthic boundary layer. In *The Sea*, volume 4, pages 731–758. Wiley.